applied sciences

MDPI

Article

Mechanical and Energy Evolution Characteristics of Sandstone under True Triaxial Cyclic Loading

Chunliang Dong [1,2], Chaotao Fan [1,3,*], Xiaoyu Lu [1,2], Guangming Zhao [1,4], Minjie Qi [1,4] and Ruipeng Qin [3]

[1] State Key Laboratory of Mining Response and Disaster Prevention and Control in Deep Coal Mines, Anhui University of Science and Technology, Huainan 232001, China; dongchunliang@163.com (C.D.); luxy@aust.edu.cn (X.L.); zhaogm@aust.edu.cn (G.Z.); 18755788657@163.com (M.Q.)
[2] School of Mechanics and Optoelectronics Physics, Anhui University of Science and Technology, Huainan 232001, China
[3] School of Civil Engineering and Architecture, Anhui University of Science and Technology, Huainan 232001, China; austqin@163.com
[4] School of Mines, Anhui University of Science and Technology, Huainan 232001, China
* Correspondence: fanchaotaogq@163.com; Tel.: +86-187-558-724-83

Abstract: To study the mechanical and energy evolution characteristics of sandstone under true triaxial cyclic loading, a sandstone mechanical test with different intermediate principal stress under true triaxial loading was conducted using the rock true triaxial disturbance unloading test system. The influence of axial load on the deformation, energy evolution, and macroscopic failure characteristics of sandstone under different intermediate principal stress in a true triaxial test was systematically analyzed, and the damage evolution law of sandstone under true triaxial cyclic load was revealed. Results showed that the failure mode of sandstone under true triaxial compression changed from tension–shear composite failure to tension failure. Grading cyclic load σ_1 greatly influenced maximum principal strain ε_1 and minimum principal strain ε_3 but had little influence on intermediate principal strain ε_2. Under the same σ_2 condition, the input energy and elastic energy in σ_1, σ_2, and σ_3 directions increased nonlinearly. Under different σ_2 conditions, the dissipated energy in σ_1, σ_2, and σ_3 directions decreased with the increase in σ_2. With the increase in σ_2, graded cycles σ_1, ε_2, and ε_3 decreased considerably, and the failure mode changed from tensile failure to shear failure. When the cyclic loading rate increased, the σ_1, ε_1, ε_2, ε_3, and volume strain ε_v of sandstone failure decreased, but the expansion point increased. Under true triaxial grading cyclic loading and unloading, the total dissipated energy of sandstone increased exponentially. The larger σ_2 was, the smaller the damage variable was.

Keywords: rock mechanics; true triaxial cycle; energy; deformation; damage characteristics; damage

check for updates

Citation: Dong, C.; Fan, C.; Lu, X.; Zhao, G.; Qi, M.; Qin, R. Mechanical and Energy Evolution Characteristics of Sandstone under True Triaxial Cyclic Loading. *Appl. Sci.* **2023**, *13*, 7230. https://doi.org/10.3390/app13127230

Academic Editor: Stefano Invernizzi

Received: 26 May 2023
Revised: 13 June 2023
Accepted: 14 June 2023
Published: 16 June 2023

1. Introduction

In the process of underground engineering construction, due to the interference of artificial repeated drilling, blasting, roadway excavation, support, and natural geological tectonic movement, the rock mass is often subjected to cyclic loading, and rock failure under cyclic loading is a progressive fracturing process [1–4]. In addition, in engineering activities such as mining adjacent rock strata or roadway excavation, rock mass stress increases and decreases periodically to form cyclic disturbance, which will also make the rock mass bear cyclic load or even graded cyclic load. The mechanical properties and energy evolution of rock mass under cyclic loading influence the long-term stability of underground engineering. Many domestic and foreign scholars have investigated the mechanical characteristics of rocks under cyclic loading. Yintong et al. [5] studied salt rock's deformation and damage characteristics under uniaxial cyclic loading. Xiurun et al. [6,7] conducted a uniaxial cyclic loading test and reported that rock deformation under axial cyclic loading undergoes initial, stable, and accelerated stages. Yongjie et al. [8] found that the number of cyclic loads in the process of fatigue failure of coal rocks can reflect the entire rock process from compaction and strain-hardening stages to the strain-softening stage; it can also reflect the process of damage evolution. Liu et al. [9] analyzed sandstone deformation, strength, and damage under different cyclic loading frequencies. Fuenkajorn et al. [10] examined salt rock strength, residual deformation, and elastic modulus under cyclic loading. Xiaoquan et al. [11] found that the plastic deformation of coal samples under cyclic loading is the largest in the first cycle and then gradually decreases, and the axial stress and strain are positively correlated. To further understand the mechanical and damage behavior of rock under true three-dimensional disturbance, it is necessary to study the deformation, energy dissipation, and damage evolution characteristics of rock under true triaxial cyclic loading. This will further reveal the damage mechanism of rock gradual deterioration caused by true three-dimensional cyclic disturbance, which has important guiding significance for prediction and prevention of rock dynamic disasters.

The elastic deformation, residual deformation, microcracks, and pores of rocks under load directly reflect the transfer process of energy. Therefore, studying the energy evolution of rocks under cyclic loading is essential for dynamic disaster prediction and safety evaluation of rock masses in underground engineering. Liu et al. [12] studied the relationship among the fatigue energy, fatigue deformation, and damage evolution of rocks under cyclic loading and unloading through a uniaxial cyclic loading and unloading test. Huafeng [13] investigated the evolution of sandstone's total energy, elastic energy, and dissipated energy under cyclic loading and the relationship between them. Meng et al. [14] conducted uniaxial cyclic loading and unloading tests on rocks, studied the energy accumulation and dissipation characteristics of rocks under different loading and unloading paths, and revealed the evolution and distribution of energy during rock failure. Song et al. [15] discussed the relationship between the dissipated energy and electromagnetic radiation of coal rocks under cyclic loading. Dai et al. [16] established a damage criterion based on the energy dissipation obtained from the cyclic impact load test of granite, which could well characterize the relationship between the damage and the number of impacts. Most of the above experimental studies were carried out under uniaxial or conventional triaxial conditions. However, the majority of the rock masses in underground engineering practice are in the true triaxial state ($\sigma_1 > \sigma_2 > \sigma_3$) with unequal 3D stress. Whether the rock damage and failure laws obtained through a conventional triaxial or uniaxial test are applicable to mining rock masses under the true triaxial state remains to be determined.

So far, many scholars have gradually begun studying the mechanical rock properties and energy evolution law in the true triaxial state. For example, Moji [17] carried out experimental studies on the failure effects of granite, limestone, and dolomite under different conditions, and found that had a significant effect on brittle materials. Baumgarten et al. [18] studied the failure behavior of sandstone in different types of triaxial compression tests and simulated the internal fracture mode of rock after failure by PFC3D. Finally, they proved that the grain shape had a great influence on micromechanics. Based on uniaxial tension, uniaxial compression, and biaxial compression tests, Ivan [19] proposed a new strength criterion for rock under true triaxial stress conditions, which could help reduce the effort required for experimental research and improve the mining efficiency of underground engineering. Kwaniewski et al. [20] used the improved original Mogi-type testing apparatus to study the deformation and brittle failure behavior of hard rock and the cause of rockburst. Gao et al. [21] explored the deformation, energy, and damage evolution law of marble during cyclic loading through true triaxial cyclic loading and unloading tests. Feng et al. [22] investigated the relationship between rock properties and cumulative damage and their changing rules via cyclic loading and unloading tests on rocks with different properties.

However, only a few studies have been conducted on sandstone's mechanical characteristics and energy evolution under true triaxial cyclic loading, but the influence of intermediate principal stress on rock mechanical behavior in the true triaxial state is particularly important. Therefore, this experimental research examines the mechanical and energy evolution characteristics of sandstone under different intermediate principal stresses, explores the influence of axial circulation on the deformation, energy, and damage of sandstone under different intermediate principal stresses, and reveals the mechanical characteristics, energy evolution, and damage deformation law of sandstone under true triaxial cyclic disturbance.

2. Test Equipment and Programs

2.1. Test Equipment

The Beijing Soft Island DS5 acoustic emission system and the true triaxial disturbance unloading rock test system developed by Anhui University of Science and Technology and manufactured by Changchun Chaoyang Test Instrument Co., Ltd. (Changchun, China) were used in this test (Figure 1).

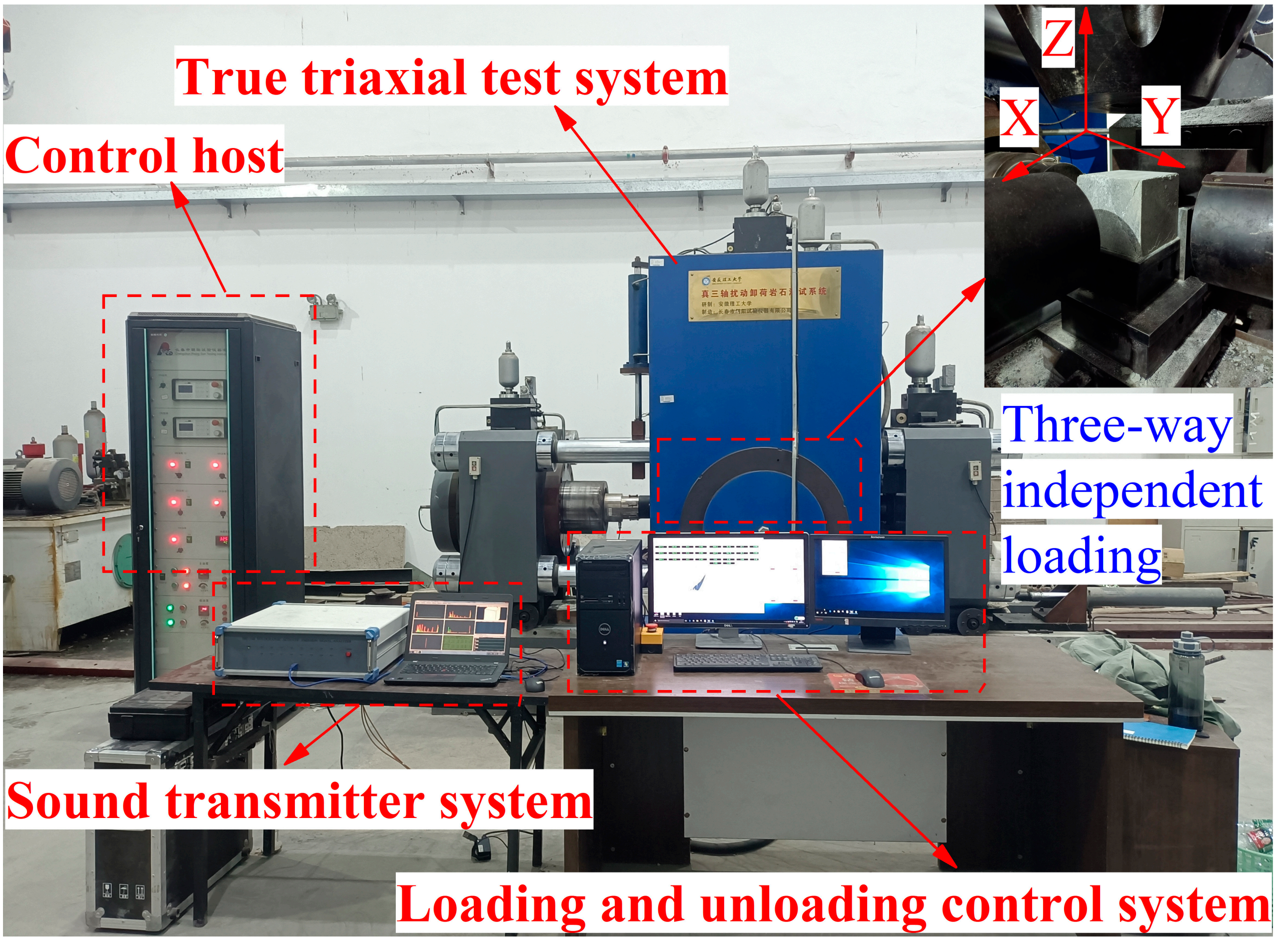

Figure 1. Rock true triaxial disturbance unloading test system and monitor.

(1) The true triaxial testing machine consists of the main loading structure, horizontal and vertical loading modules, a 3D independent loading chamber, a pressure displacement sensor, a computer that can control loading and unloading, and software that can collect and analyze data. A digital servo controller controls all three directions. A maximum pressure of 5000 kN can be applied in the vertical (Z) direction, and a maximum pressure of 3000 kN can be applied in the horizontal (X, Y) direction. The control computer can realize the displacement or stress of one-way, two-way, three-way, step, and cyclic loading as well as unloading, and an axial disturbance test was conducted to examine the real rock mass under different loading and unloading paths of mechanical properties.

(2) The acoustic emission (A.E.) monitoring system is Beijing Soft Island DS5, and it uses six A.E. probes to collect A.E. events, frequency, amplitude, energy, and other

parameters in real time. In the test, the preamplifier was set to 40 dB. To minimize the influence of external interference on the test, the noise threshold value was set to 45 dB, and the sampling frequency was set between 1 kHz and 1 MHz to monitor the damage characteristics of the rock during the test.

2.2. Test Specimens

The original rock samples in this test were sandstone specimens from the same producing area, as shown in Figure 2. The internal structure of the rock samples was similar, and the size was 100 mm × 100 mm × 100 mm. The flatness error of the end face was controlled within ±0.02 mm, and the perpendicularity error was ±0.25°. The uniaxial compressive strength of the rock sample was 62 MPa. Because of the limitation of test conditions, the porosity and particle composition of rock samples could not be tested. If conditions permit, it is recommended to measure it, as it is conducive to the rigor of the test.

Figure 2. Sandstone specimens.

2.3. Test Methods and Contents

Before the test, the cubic sandstone sample was placed in the true triaxial pressure chamber, and Vaseline was applied in advance to the acoustic emission probe, which was installed at different positions of the fixture to ensure the accuracy of the acoustic emission instrument in collecting the signal. The acoustic emission signal and the true triaxial data were collected at the same time to ensure the synchronization of time and data. The test plan parameters are shown in Table 1.

Table 1. Test scheme parameters.

Sample Number of Rock	Predetermined Load (kN)			Loading Rate (kN/min)	Unloading Rate (kN/min)
	σ_3	σ_2	σ_1		
1#	0	0	0	140	/
2#	10	20	60	140	/
3#	10	20	60	140	140
4#	10	20	60	200	200
5#	10	40	60	200	200
6#	10	60	60	200	200

Compared with the conventional triaxial cyclic loading test [23,24], the true triaxial cyclic loading test is more in line with the mechanical state of rocks in the process of rock excavation in practical engineering. The mechanical behavior of rocks differs due to different excavation speeds or rock stress states. Therefore, the true triaxial axial compression and true triaxial axial cyclic load tests in this study were designed to simulate the influence of true triaxial cyclic excavation disturbance on the mechanical behavior of sandstone. The load stress path of sandstone in the true triaxial state is shown in Figure 3. The test scheme and steps are as follows:

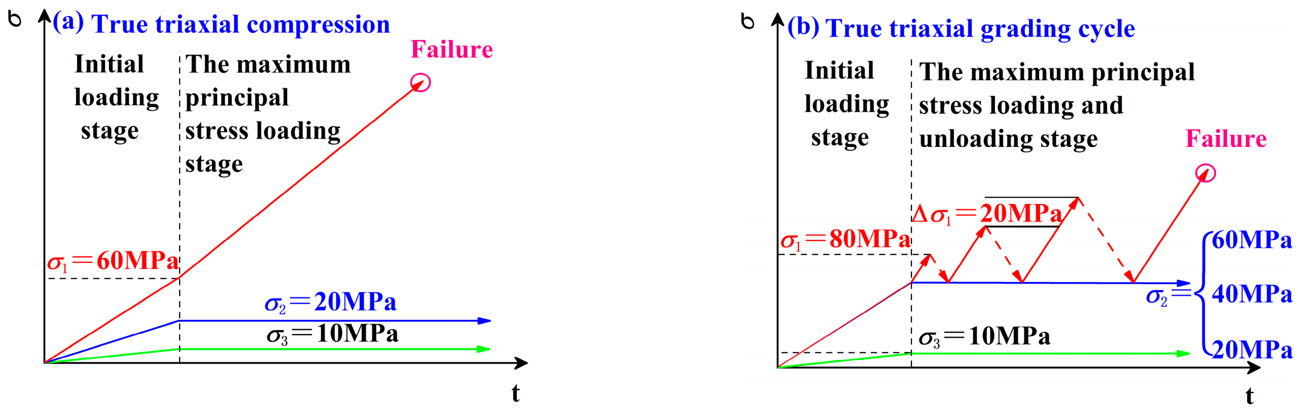

Figure 3. True triaxial axial load stress paths.

Scheme 1: The loading rate was 140 kN/min, and σ_1 (Z) was loaded until specimen failure.

Scheme 2: Each principal stress reached the predetermined load at a constant loading rate, and σ_2 (Y direction) and σ_3 (X direction) were unchanged. σ_1 was loaded at a rate of 140 kN/min until the specimen was destabilized. The stress path is shown in Figure 3a.

Scheme 3: The predetermined load was applied, and σ_2 and σ_3 were unchanged (similar to Scheme 2). Next, a 140 kN/min rate grading cycle of loading and unloading (σ_1) was applied, and each level of stress increment was 20 MPa. The stress path is shown in Figure 3b.

Scheme 4: Loading to the predetermined load was performed, and σ_2 and σ_3 were unchanged (similar to Scheme 2). Next, a 200 kN/min rate grading cycle of loading and unloading (σ_1) was performed, and the loading at each stage was increased by 20 MPa. The stress path is shown in Figure 3b.

3. Test Results and Analysis

3.1. Analysis of Deformation and Failure Characteristics of Specimens

The mechanical parameters in different principal stress directions change with the change in the principal stress state due to the anisotropy of rock mass and its properties. In addition, with the change in the load path and rate, the deformation and failure characteristics of rock mass present great differences.

3.1.1. Strength and Deformation Analysis of Sandstone under Different Stress Paths

Figure 4 shows the axial stress–strain curves of sandstone under different stress paths. In the uniaxial compression test, the stress–strain curve of sandstone changed nonlinearly. After reaching the peak stress, the bearing capacity of sandstone decreased instantaneously, and apparent brittle failure occurred. By contrast, sandstone showed an inevitable ductile failure after reaching the peak stress in the true triaxial state because the existence of confining pressure enabled sandstone to absorb abundant energy before failure and effectively limited the radial deformation of sandstone.

The rock under the three stress paths experienced the compaction stage (I), the elastic stage (II), and the ductile stage (III). The rock also experienced the post-peak failure stage (IV) in the true triaxial state. The post-peak failure stage under uniaxial compression was not obvious, and the axial stress–strain curve of sandstone was in the true triaxial state. The stress at each stage was higher than that under uniaxial compression, indicating that the existence of confining pressure reduced the severity of rock failure and greatly improved the strength of the rock. In addition, the peak stress of sandstone under the true triaxial state differed. The peak stress of sandstone under true triaxial compression was higher than that under true triaxial cyclic loading, because in the process of graded cyclic loading and unloading, the original pores and cracks were cyclically closed and expanded under axial load. New cracks were generated simultaneously, so the sandstone under true triaxial cyclic loading was prone to damage and instability failure. In addition, the elastic stage of sandstone under true triaxial compression was longer than that under true triaxial cyclic loading.

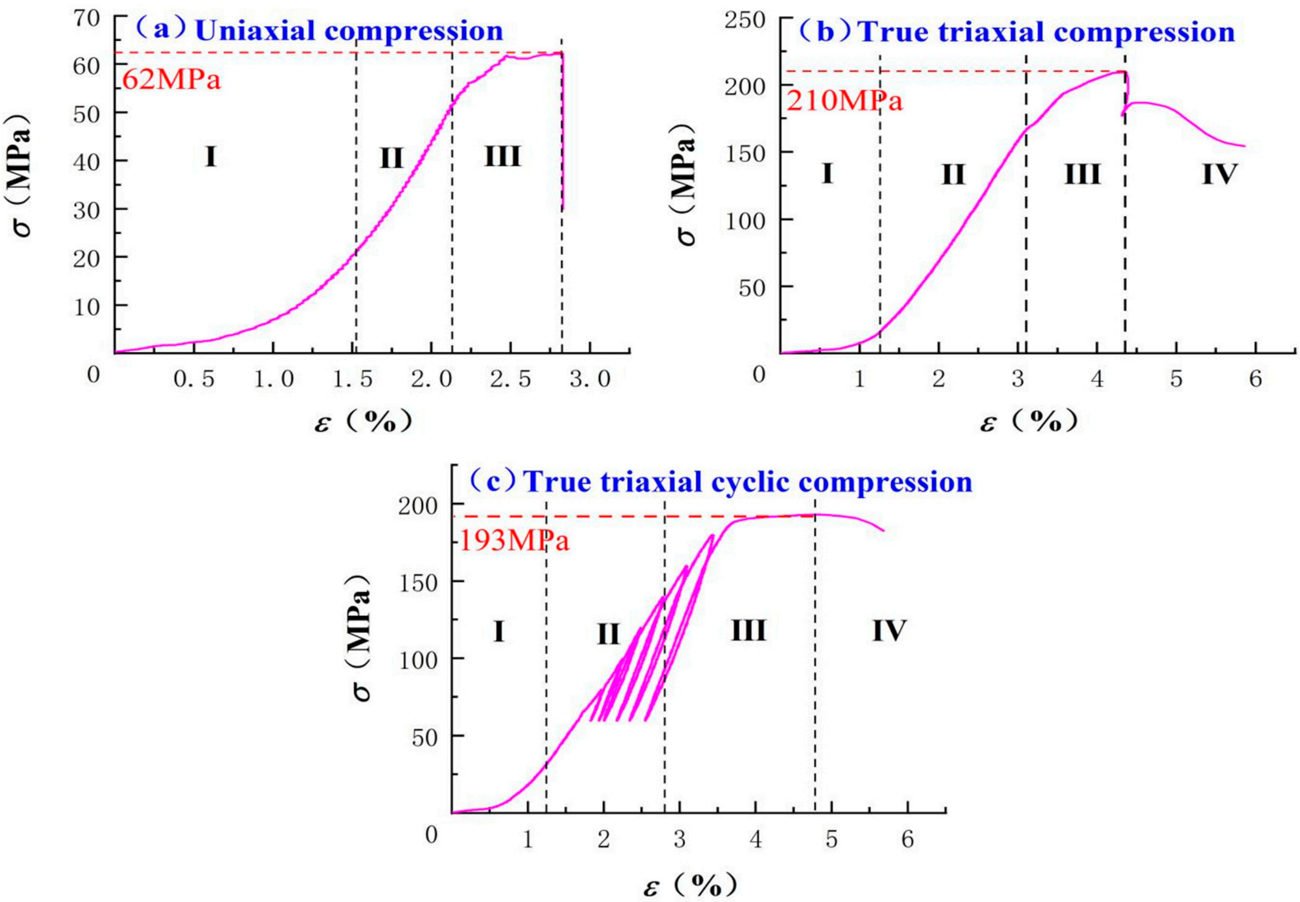

Figure 4. Axial stress–strain curves under different stress paths.

3.1.2. Analysis of Sandstone Failure Characteristics under Different Stress Paths

The macroscopic failure characteristics of sandstone under different stress paths are shown in Figure 5. In this study, the results of the uniaxial compression test, true triaxial compression test, and true triaxial cyclic test under the same conditions were adopted as examples to further describe the different macroscopic failure characteristics of sandstone under different stress paths.

The diagram indicates that the failure state, crack development degree, and failure mode of sandstone differed under the three stress paths. Under uniaxial compression, the reaction of sandstone failure was severe, and the inverted V-shaped shear crack was completely penetrated to cause instability failure. The crack development was sufficient, showing obvious brittle failure characteristics. Under true triaxial compression, sandstone was mainly dominated by tension–shear composite failure, and tensile cracks were observed near the minimum principal stress surface. The cracks were fully developed. Under true triaxial cyclic loading, many incompletely developed non-interpenetrated cracks far from the minimum principal stress plane were found in sandstone. Near the minimum principal stress plane, several tensile cracks that were nearly perpendicular to the maximum principal stress plane were formed and finally split into rock plates. Under the different stress paths, the development patterns of the cracks differed when sandstone was damaged. Uniaxial compression was beneficial to the formation of shear cracks; true triaxial compression was beneficial to the formation of tensile–shear cracks, and the true triaxial cycle was beneficial to the formation of tensile cracks, resulting in differences in macroscopic failure characteristics.

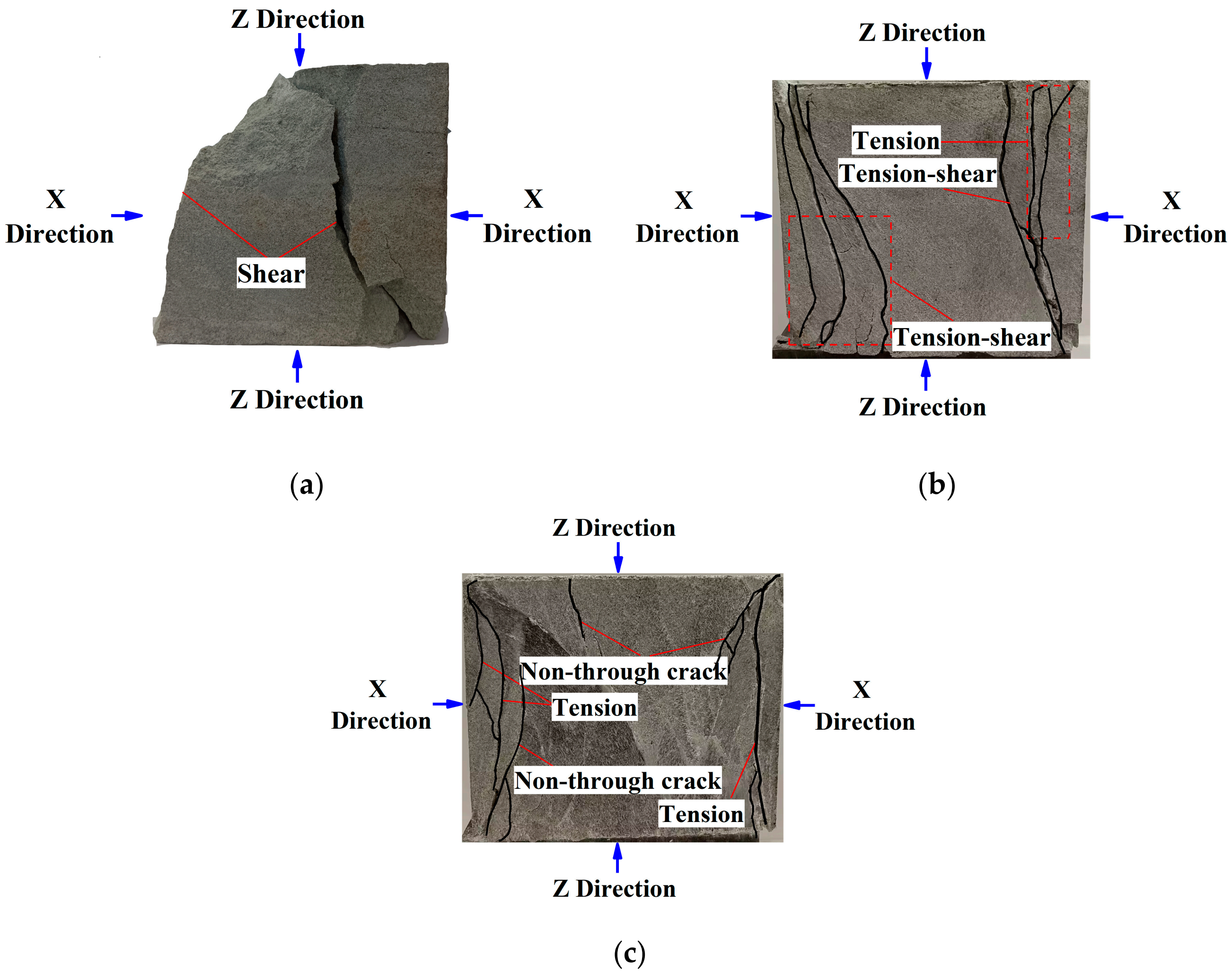

Figure 5. Failure characteristics of sandstone under different stress paths. (**a**) Uniaxial compression, (**b**) true triaxial compression, (**c**) true triaxial cyclic compression.

3.1.3. Strength and Deformation Analysis of Sandstone under Graded Cyclic Loading σ_1

Given that this group of tests refers to the process of studying cyclic load σ_1, the preloading stage before the load reached the predetermined value was not the focus of this study. To comprehensively analyze the deformation, hysteresis loop, and permanent deformation in each principal stress direction during true triaxial cyclic loading, the predetermined loading point was regarded as the zero point of deformation. Figure 6 shows the stress–strain curve of the effect of step cyclic loading σ_1 on maximum principal strain ε_1, medium principal strain ε_2, and minimum principal strain ε_3. The results showed that σ_1 cyclic loading and unloading exerted the greatest influence on sandstone ε_1, followed by ε_3. ε_2 was influenced the least, indicating that the σ_1 and σ_3 directions were the dominant deformation directions when true triaxial cyclic load σ_1 was applied.

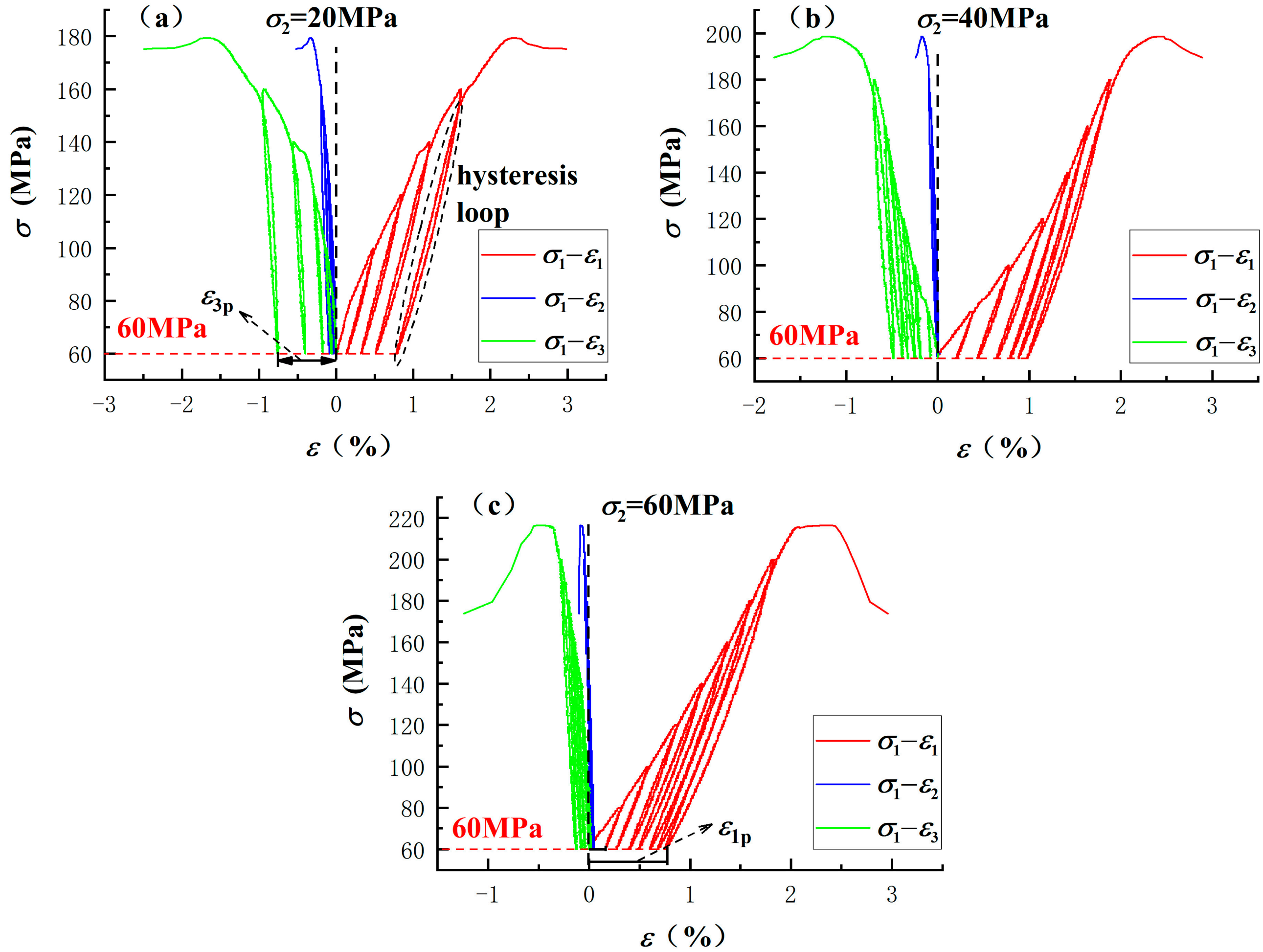

Figure 6. Cyclic σ_1 stress–strain curves under different σ_2 conditions.

Under the same σ_2 condition, the unloading curve of the previous level and the loading curve of the next level were closed, thus forming a hysteresis loop. With graded cyclic loading and unloading σ_1, the $\sigma_1 - \varepsilon_1$ and $\sigma_1 - \varepsilon_3$ curves gradually increased in a spiral shape, and obvious permanent deformation (ε_{1p}, ε_{3p}) characteristics were noted. During each cyclic loading σ_1, when the loading stress exceeded the unloading point of the previous stage, the deformation curve continued to rise along the loading curve of the previous stage, indicating that the rock deformation had memory characteristics at the elastic stage [25,26].

Under different σ_2 conditions, the stress–strain curves in the process of graded cyclic load σ_1 were different. As shown in Figure 6a, when σ_2 was small, the deformation of sandstone in the three principal stress directions was large. With the increase in σ_2, cyclic load σ_1 reduced ε_2 and ε_3 considerably, especially ε_2, and the strength of the rock under the true triaxial state increased, as shown in Figure 6b,c. When σ_2 was small, the deviatoric stress ($\sigma_2 - \sigma_3$) was small, and the cyclic load caused large compression deformation in this direction and large expansion deformation in the σ_2 and σ_3 directions. When σ_2 increased, the deviatoric stress ($\sigma_2 - \sigma_3$) was large, and σ_2 inhibited the deformation in the σ_1 direction and the development of rock fissures, leading to a decrease in ε_2 and ε_3 and an increase in rock peak stress. However, studies have shown that large deviatoric stress ($\sigma_2 - \sigma_3$) promotes the σ_3 direction to produce large expansion deformation [27].

The deformation trends of sandstone under different loading and unloading rates in the true triaxial state were the same, as shown in Figure 7. With the increase in the loading and unloading rate, the σ_1, ε_2, ε_3, and ε_v of sandstone failure decreased. In the process of grading cyclic loading and unloading σ_1 of sandstone, the cracks between the internal grains continued to open and close. When the load rate increased, the cracks generated inside were not completely closed, and new cracks were produced, resulting in a reduction in the energy required for crack development and the acceleration of crack propagation. When the sandstone was destroyed, the maximum load that could be borne in the σ_1 direction was small, and the deformation in the σ_1 direction was reduced, so the deformation in the σ_2 and the σ_3 directions was also reduced. Figure 7c indicates that the rock expanded during damage, and the expansion point appeared in advance with the increase in the loading and unloading rate. When the rock was damaged, the expansion characteristics became increasingly obvious, indicating that under the condition of true triaxial graded cyclic load σ_1, the loading rate played a leading role in the expansion of the rock.

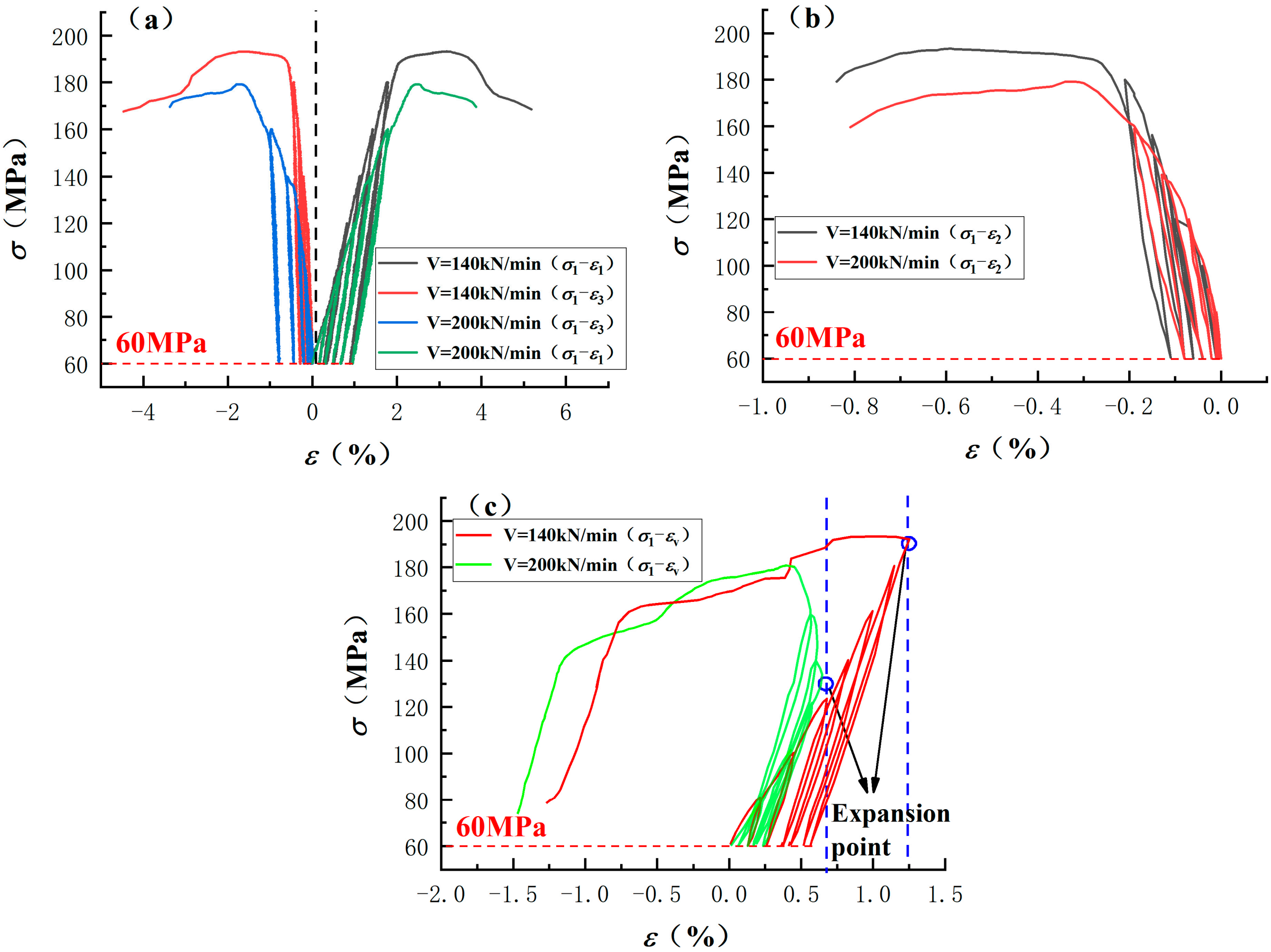

Figure 7. Stress–strain curves of sandstone under different true triaxial loading rates. (**a**) σ_2 = 20 MPa, (**b**) σ_2 = 20 MPa, (**c**) σ_2 = 20 MPa.

3.1.4. Analysis of Acoustic Emission and Failure Characteristics of Sandstone under Graded Cyclic Loading σ_1

The microscopic failure (cracks, fissures, etc.) inside a rock is closely related to its external macroscopic failure form. Acoustic emission can detect the energy accumulated and released by the microscopic fracture of rocks under the action of external force and can send signals in the form of a stress wave. However, the energy released by the development and closure of rock cracks and pores under different load conditions differs greatly, resulting in different macroscopic damage phenomena [28]. Therefore, the internal relationship between acoustic emission characteristics and macroscopic failure phenomena can be established by combining acoustic emission parameters, such as ringing count and energy, as shown in Figure 8.

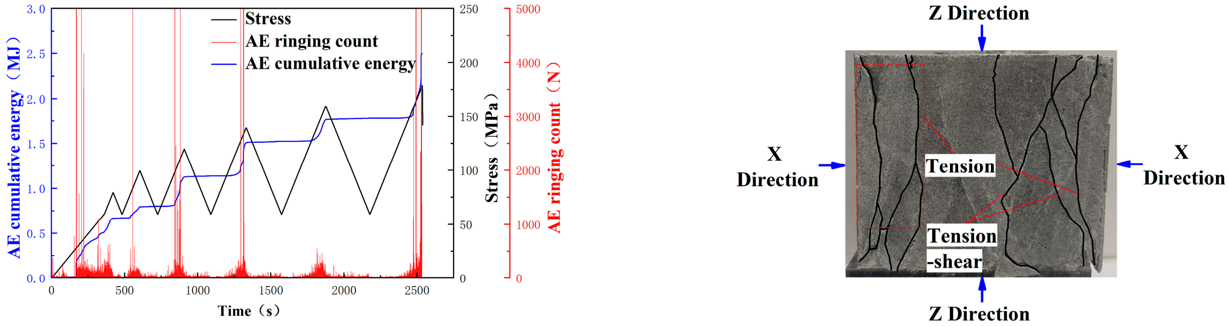

(**a**)

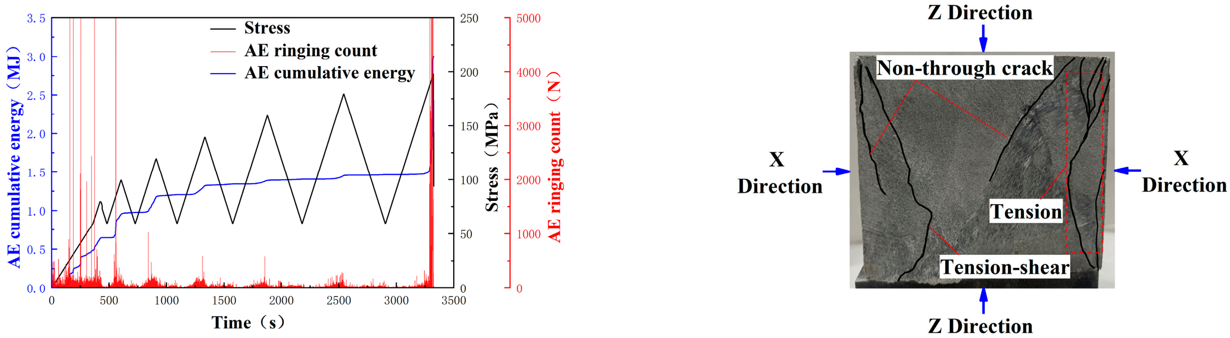

(**b**)

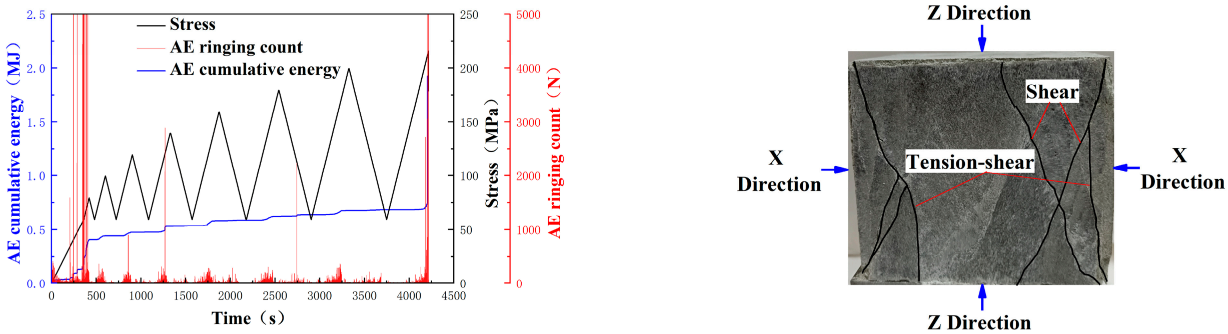

(**c**)

Figure 8. Acoustic emission and failure characteristics of rock under different σ_2 conditions. (**a**) σ_2 = 20 MP, (**b**) σ_2 = 40 MP, (**c**) σ_2 = 60 MP.

In this study, the acoustic emission characteristics of sandstone under different σ_2 conditions were generally similar and could be divided into active, quiet, and explosion periods. In the active period, the sandstone entered the compaction stage, the primary pores and cracks inside the rock were closed under the action of stress, and the mutual friction between the internal grains produced abundant acoustic emission signals. The rock entered the quiet period of acoustic emission signal after compaction. At this stage, acoustic emission signals appeared in each loading and unloading cycle, but the acoustic emission signals were relatively few and stable, indicating that the cracks in the rock were developing steadily. The acoustic emission during the unloading process was small because the microstructure of the rock rebounded and opened during the unloading failure process, so the acoustic emission signal during the quiet period was mainly concentrated in the loading part. The sudden increase in acoustic emission signals in the explosion period indicated that the rock entered the failure stage, and the internal cracks and pores developed rapidly and produced new cracks at the same time. The new and old cracks interlaced with each other to form macroscopic failure.

Figure 8 shows that the cumulative energy of acoustic emission under the different σ_2 conditions had a consistent upward trend, and the increase in each energy was closely related to the microscopic damage inside the rock. The smaller σ_2 was, the greater the increase was in each loading energy and cumulative A.E. energy before the rock was destroyed. When σ_2 = 20 MPa, the sandstone formed a failure feature dominated by tension and supplemented by a tension–shear composite. In the macroscopic state, additional tension and shear cracks were formed, and the damage was severe, accompanied by a large amount of debris. This situation corresponded to the high energy increase during the loading process and the large cumulative A.E. energy value before failure. When σ_2 = 40 MPa, the sandstone was dominated by tension–shear composite failure accompanied by incomplete non-through cracks, and tensile and tensile–shear cracks were formed in the macro state. When σ_2 = 60 MPa, the sandstone was mainly dominated by shear failure, and few shear and tensile–shear cracks were formed in the macro state, which corresponded to the low energy increase during the loading process and the small cumulative A.E. energy value before failure. Therefore, the acoustic emission signal had good correspondence with the macroscopic failure characteristics of the rock. The internal failure law of the rock could be analyzed using acoustic emission parameters, and the macroscopic failure mode of the rock could be inferred, which is important for the design and support of engineered underground rock mass.

3.2. Analysis of Energy Evolution and Damage Characteristics of Sandstone True Triaxial Loading and Unloading under Different σ_2 Conditions

3.2.1. Definition of Rock Energy Parameters in the True Triaxial State

The deformation and damage of rocks under external force are essentially processes of internal energy release and dissipation. In a rock mechanics test, the total input energy of the external load on the rock is partly stored in the rock mass in the form of elastic energy and partly dissipated in various forms. Assuming that the rock unit has no heat exchange with the outside world during the action of external force, the deformation of the rock unit under the action of external force conforms to the first law of thermodynamics [29–34], that is,

$$U = U_e + U_d, \tag{1}$$

where U is the total input energy generated by the external force of the unit, U_e is the total elastic energy that the unit can release, and U_d is the total dissipated energy of the unit.

In a true triaxial axial graded cyclic loading test, the energy input of rock mass can be divided into two parts: axial input energy and circumferential input energy [25,35]. Therefore, the total energy input per unit volume of external force can be defined as

$$U = U_1 + U_2 + U_3, \tag{2}$$

where U_1, U_2, and U_3 are the energy inputted by the maximum, medium, and minimum principal stresses, respectively, to deform the specimen.

In a graded cyclic loading test, each level of stress has corresponding upper and lower limits for carrying out regular cyclic loading and unloading. The hysteresis curve during the cycle is often not closed due to the existence of rock damage [36,37]. In this study, the relationship between axial input energy and dissipated energy was illustrated by the i-cyclic stress–strain hysteresis curve during cyclic loading and unloading. As shown in Figure 9a, the area surrounded by ABB′A′ is the energy $u_{1,i}$ inputted by the axial stress to the sandstone during the i-cycle loading process, the area surrounded by CBB′C′ is the energy $u_{1,i}^e$ released by the sandstone during the i-cycle unloading process, and the area surrounded by ABCC′A′ is the energy $u_{1,i}^d$ dissipated by the sandstone during the i-cycle unloading process. Following the definition of calculus, the maximum principal stress input total energy U_1 of the loading part during the whole cycle, the total energy U_{1e}

released by the unloading part, and the total energy U_{1u} dissipated during the cycle can be obtained as follows:

$$U_1 = \sum_{i=1}^{z} \int_{\varepsilon_{1,i}}^{\varepsilon_{1,i}^e} \sigma_1 d_{\varepsilon_1}, \tag{3}$$

$$U_{1e} = \sum_{i=1}^{z} \int_{\varepsilon_{1,i}^u}^{\varepsilon_{1,i}^e} \sigma_1 d_{\varepsilon_1}, \tag{4}$$

$$U_{1d} = U_1 - U_{1e}, \tag{5}$$

where σ_1 and ε_1 are axial stress and strain, respectively; $\varepsilon_{1,i}$ is the axial strain corresponding to the starting point of *i*-cyclic loading; $\varepsilon_{1,i}^e$ is the axial strain corresponding to the upper limit of *i*-cyclic loading; $\varepsilon_{1,i}^u$ is the axial strain corresponding to the lower limit of *i*-cyclic unloading; and z ($z = 1, 2, \cdots,$) is the maximum number of cycles.

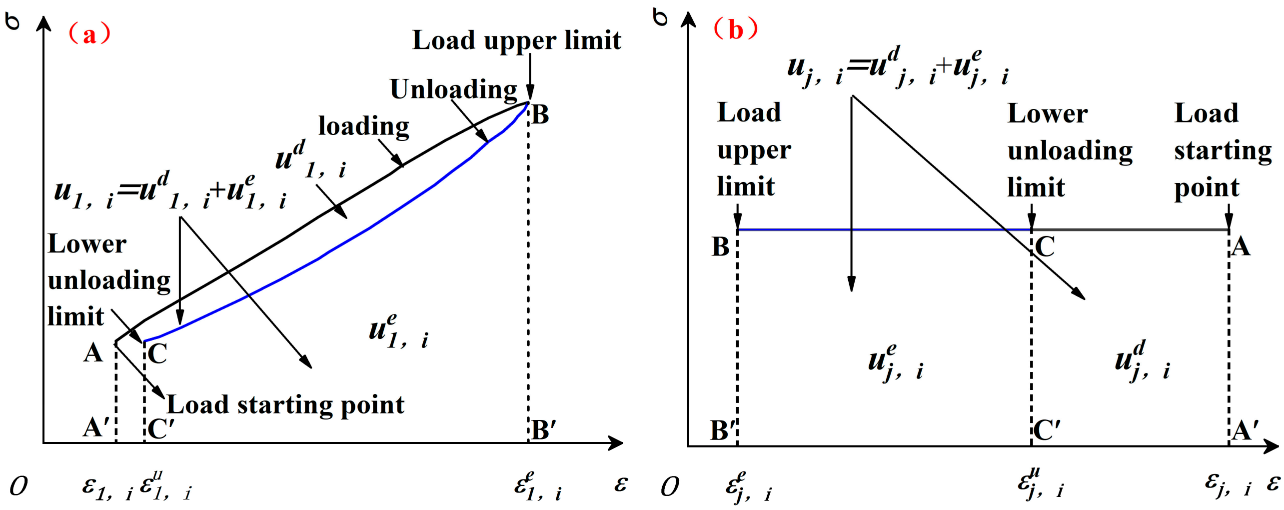

Figure 9. Energy principle diagram of true triaxial cyclic loading and unloading. (**a**) Axial direction, (**b**) circumferential directions.

As shown in Figure 9b, the intermediate principal stress and the minimum principal stress remain constant throughout the cycle. The area surrounded by ABB′A′ is the energy $u_{j,i}$ inputted by the radial stress to the sandstone during the *i*-cycle loading process. The area surrounded by CBB′C′ is the energy ($u_{j,i}^e$) released by the sandstone in the radial direction during the *i*-cycle unloading process. The area surrounded by ACC′A′ is the radial dissipated energy $u_{j,i}^d$ of sandstone during the *i*-cyclic loading and unloading process. Total energy U_j is inputted by the radial stress of the loading part, total energy U_{je} is released by the unloading part, and total energy U_{jd} is dissipated during the cycle. The formula is as follows:

$$U_j = \sum_{i=1}^{z} u_{j,i} = \sum_{i=1}^{z} \left[\sigma_j \left(\varepsilon_{j,i}^e - \varepsilon_{j,i}\right)\right], \tag{6}$$

$$U_{je} = \sum_{i=1}^{z} u_{j,i}^e = \sum_{i=1}^{z} \left[\sigma_j \left(\varepsilon_{j,i}^u - \varepsilon_{j,i}^e\right)\right], \tag{7}$$

$$U_{jd} = \sum_{i=1}^{z} u_{j,i}^d = |U_j| - |U_{je}|, \tag{8}$$

where σ_j (j = 2, 3) is the j principal stress, $\varepsilon_{j,i}$ is the strain corresponding to the j principal stress at the starting point of the *i*-cyclic loading, $\varepsilon_{j,i}^e$ is the strain corresponding to the j

principal stress at the upper limit of the i-cyclic loading, and $\varepsilon_{j,i}^{u}$ is the strain corresponding to the j principal stress at the lower limit of the i-cyclic unloading.

3.2.2. Energy Evolution Law of Maximum Principal Stress Direction under Different σ_2 Conditions

Deformation and failure occur when a rock is subjected to external force in a true triaxial state accompanied by energy accumulation and dissipation. The specific values of energy in each principal stress direction of the rock under true triaxial cyclic loading can be obtained using the abovementioned energy parameter definition method. In this study, by comparing the energy accumulation and dissipation in the rock in each principal stress direction under true triaxial cyclic loading, the energy evolution law of the rock under different σ_2 conditions was analyzed. A true triaxial cyclic loading test was conducted using the energy analysis method in the true triaxial compression and uniaxial graded loading and unloading test of Zhixi et al. [38]. With the linear energy storage law proposed by Fengqiang et al. [39–41], the energy evolution law in the true triaxial cyclic loading test of sandstone was analyzed. In addition, to facilitate the analysis, energy density (kJ·m^{-3}) was utilized to represent the energy per unit volume of rock. The energy calculation results for each principal stress direction under true triaxial cyclic loading and unloading under different σ_2 conditions are shown in Table 2.

The axial input energy–stress, elastic energy–stress, and dissipated energy–stress curves under different σ_2 conditions are plotted in Figure 10, with the axial loading upper limit stress of single-cycle loading and unloading as the abscissa.

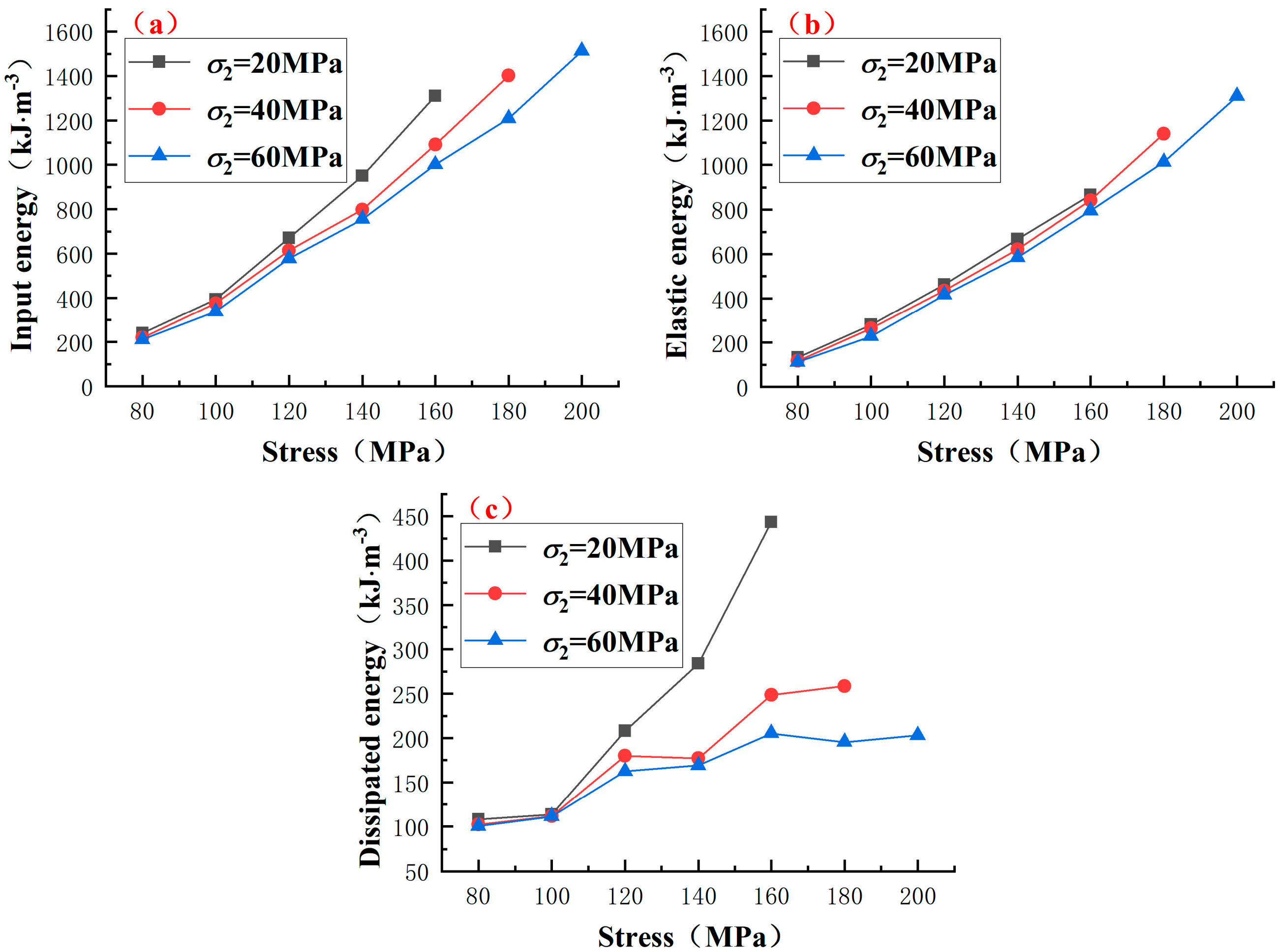

Figure 10. Axial energy-stress curves under different σ_2 conditions. (**a**) Axial input energy, (**b**) axial elastic energy, (**c**) axial dissipated energy.

Table 2. Energy values of principal stress directions under true triaxial cyclic loading and unloading under different σ_2 conditions.

Cycle Index/N	$u_{1,i}$ (kJ·m^{-3})			$u_{2,i}$ (kJ·m^{-3})			$u_{3,i}$ (kJ·m^{-3})			$u^d_{1,i}$ (kJ·m^{-3})			$u^d_{2,i}$ (kJ·m^{-3})			$u^d_{3,i}$ (kJ·m^{-3})		
	20	40	60	20	40	60	20	40	60	20	40	60	20	40	60	20	40	60
1	240.31	219.93	212	4	4	6	10	8	3	108.37	102.48	100.6	0	0	0	5	4	0
2	394.68	376.3	338.3	8	12	12	16	12	4	113.86	112.06	111.3	2	0	0	7	5	0
3	670.73	614.8	577.8	14	16	18	23	18	7	207.88	180.03	162.4	2	0	−6	11	8	0
4	950.07	799.17	755.4	22	23	24	40	24	9	283.99	177.29	169.2	4	1	0	24	10	1
5	1309.25	1090.47	1000.25	30	32	36	54	26	14	443.5	248.58	205.33	8	0	0	33	6	4
6	/	1401.21	1209.48	/	36	42	/	41	17	/	258.65	195.22	/	0	0	/	18	4
7	/	/	1512.14	/	/	48	/	/	20	/	/	202.89	/	/	0	/	/	5

With the increase in stress, the axial input energy, dissipation energy, and elastic energy of sandstone generally showed nonlinear growth, and the larger σ_2 was, the smaller the axial input energy, elastic energy, and dissipation energy were, indicating that the different σ_2 values had a great influence on the energy storage and dissipation of the rock in unit volume under the true triaxial state. Under the same σ_2, the elastic energy of the rock at each loading upper limit of axial stress was much larger than the dissipation energy, revealing that the elastic energy of the rock was higher than the dissipation energy during cyclic loading.

Under different σ_2 values, the larger σ_2 was, the smaller the dissipation energy that corresponded to the upper limit points of axial stress at all levels, and the gentler the change in unit volume dissipation energy with stress. This result indicates that a large σ_2 resulted in an obvious inhibition effect on rock failure under true triaxial cyclic loading. In the 3D stress state, a large amount of energy was stored inside the rock. During the excavation process, the rock mass released a large amount of elastic energy under the cyclic loading and unloading of external forces, which easily caused dynamic damage to the rock mass. Therefore, the study of rock energy evolution under true triaxial cyclic loading has guiding significance for the safety evaluation of rock mass excavation.

3.2.3. Energy Evolution Law of Medium and Minimum Principal Stress Directions under Different σ_2 Conditions

In the process of rock damage and failure under the true triaxial state, the intermediate principal stress and the minimum principal stress can inhibit the deformation and failure of the rock to a certain extent, but deformation still occurs; that is, energy accumulation and release still exist. With Formulas (6)–(8), the input energy, elastic energy, and dissipation energy of the single loading and unloading section can be obtained. With the axial loading upper limit stress of single-cycle loading and unloading as the abscissa, the input energy–stress, elastic energy–stress, and dissipation energy–stress curves in the direction of intermediate principal stress and minimum principal stress under different σ_2 conditions were plotted to explore the energy evolution law in the direction of intermediate principal stress and minimum principal stress under different σ_2 conditions, as shown in Figures 11 and 12.

The input energy and elastic energy of sandstone in the direction of intermediate principal stress and minimum principal stress increased with the increase in axial stress, but the energy changes in the direction of intermediate principal stress and minimum principal stress differed under the different σ_2 conditions. The larger σ_2 was, the greater the input energy and elastic energy were in the direction of intermediate principal stress but the smaller the dissipation energy was. With the increase in axial stress, the grains inside the rock slipped, and the intermediate principal stress could inhibit the deformation of the grains inside the rock in the direction of the intermediate principal stress. The larger σ_2 was, the stronger the permanent deformation ability was in the direction of the intermediate principal stress, and the more the permanent deformation of the rock was inhibited. Therefore, with the increase in σ_2, the dissipation energy in the direction of intermediate principal stress was small. When σ_2 = 60 MPa, no dissipation energy was observed in the direction of intermediate principal stress, indicating that the larger σ_2

was, the more input energy in the direction of intermediate stress was converted into elastic energy.

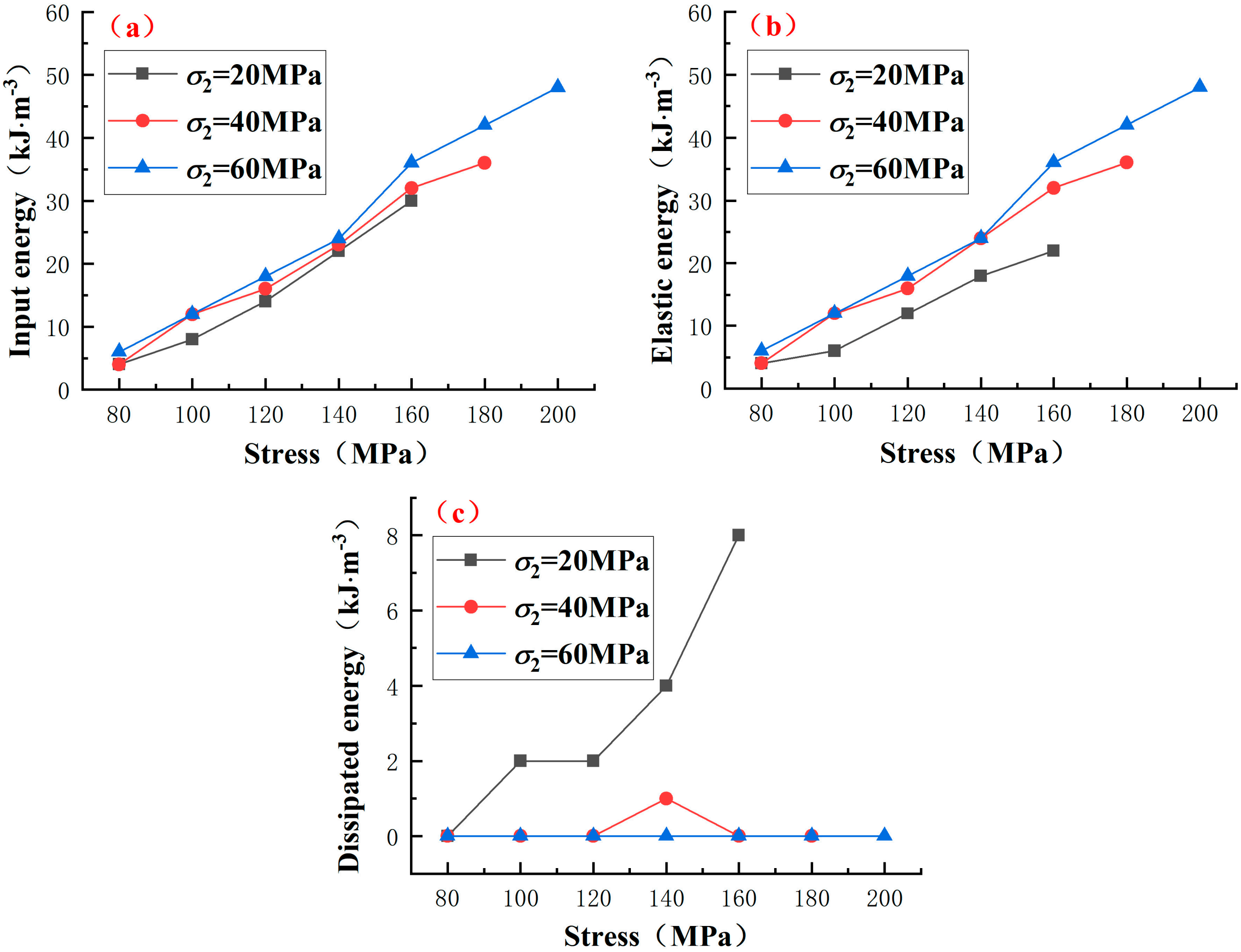

Figure 11. Energy-stress curves of intermediate principal stress direction under different σ_2 conditions. (**a**) Input energy in σ_2 direction, (**b**) elastic energy in σ_2 direction, (**c**) dissipated energy in σ_2 direction.

Compared with the intermediate principal stress, the input energy, elastic energy, and dissipation energy in the direction of the minimum principal stress decreased with the increase in σ_2 because the principal stress in the rock also had an inhibitory effect on the permanent deformation in the direction of the minimum principal stress during the true triaxial cyclic loading process. The larger σ_2 was, the more obvious the inhibitory effect was, and the smaller the input energy, elastic energy, and dissipation energy were in the direction of the minimum principal stress.

Under the same σ_2 condition, the ratio of dissipated energy to input energy (energy dissipation ratio) in the direction of the minimum principal stress was generally greater than that in the direction of the intermediate principal stress, because under the same σ_2 condition, the minimum principal stress had a weaker ability to inhibit grain slip than that in the direction of the intermediate principal stress; thus, a larger irreversible deformation occurred in the direction of the minimum principal stress. In the process of each principal stress inhibiting the internal grain slip in the rock, the large principal stress equated to a great ability to inhibit the permanent deformation of the rock, and the permanent deformation of the rock was remarkably inhibited. Therefore, compared with the dissipation energy in the direction of the intermediate principal stress, the dissipation energy in the direction of the minimum principal stress accounted for a larger proportion of the input energy, as shown in Figure 13.

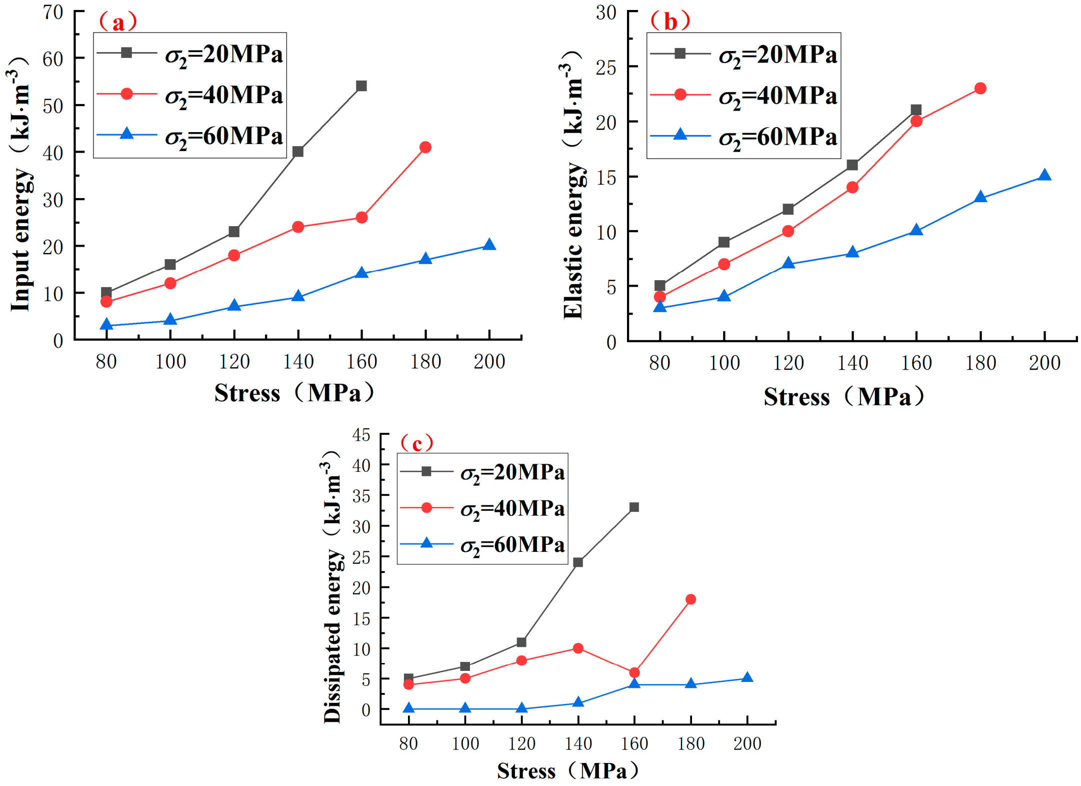

Figure 12. Energy-stress curves of minimum principal stress direction under different σ_2 conditions. (**a**) Input energy in σ_3 direction, (**b**) elastic energy in σ_3 direction, (**c**) dissipated energy in σ_3 direction.

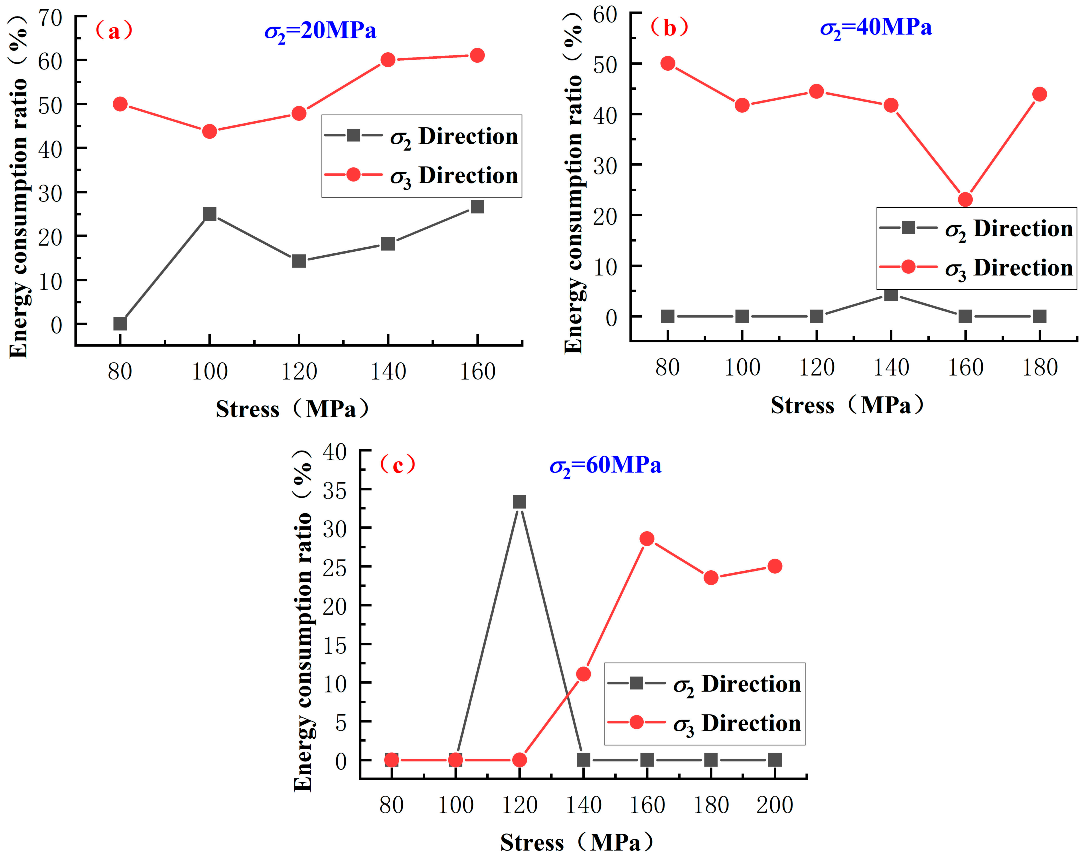

Figure 13. Medium and minimum principal stress energy consumption ratio under the same σ_2 condition.

3.3. Dissipative Energy and Damage Evolution Law of Sandstone under Different Intermediate Principal Stresses

With Formula (8), the dissipated energy in the cyclic process of sandstone under different intermediate principal stresses can be obtained. Total dissipated energy U_d can be derived by accumulating the dissipated energy in each cycle, as shown in Figure 14. The figure indicates that the cumulative dissipated energy of sandstone increased exponentially with the increase in the axial stress of sandstone, because in the graded cyclic loading and unloading, the intermediate principal stress and the minimum principal stress were unchanged. As the axial stress continued to increase, cracks and permanent deformation continued to occur inside the rock mass, which increased the energy dissipated inside the rock mass. The fitting of cumulative dissipated energy and axial stress with an exponential function can be expressed as

$$U_d = a\exp(b\sigma_1), \quad (9)$$

where U_d is the total dissipation energy, and a and b are fitting coefficients.

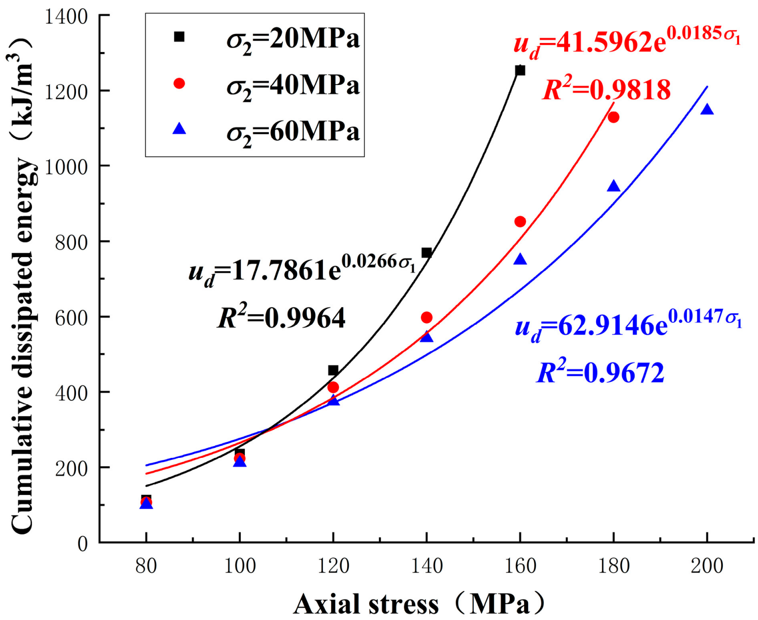

Figure 14. Accumulative dissipated energy of sandstone.

To analyze the damage characteristics of coal rock under true triaxial cyclic loading, in accordance with the damage variable of rock mass under triaxial cyclic loading and unloading proposed by Ruidong et al. [42], the expression of dissipation energy damage variable at each stress point of sandstone can be obtained as

$$D = \frac{2}{\pi}\arctan\frac{\Delta U_d}{\Delta\sigma}, \quad (10)$$

where $\Delta\sigma$ is the axial stress increment and ΔU_d is the cumulative dissipated energy increment of the corresponding point. When ΔU_d = 0, the rock mass is not damaged, and D = 0. When $\Delta U_d \to \infty$, rock damage is extremely serious, and D = 1.

In practice, the increment in dissipated energy after rock damage cannot be infinite. If the stress reaches a critical value, the rock mass will be damaged. When the axial stress exceeds the peak stress corresponding to the failure point, the rock mass is destroyed, and the damage variable corresponding to the failure point is the critical damage variable D_c. When $D \geq D_c$, the rock mass is destroyed, and the critical damage variable of the rock mass differs under different intermediate principal stress conditions, as shown in Figure 15.

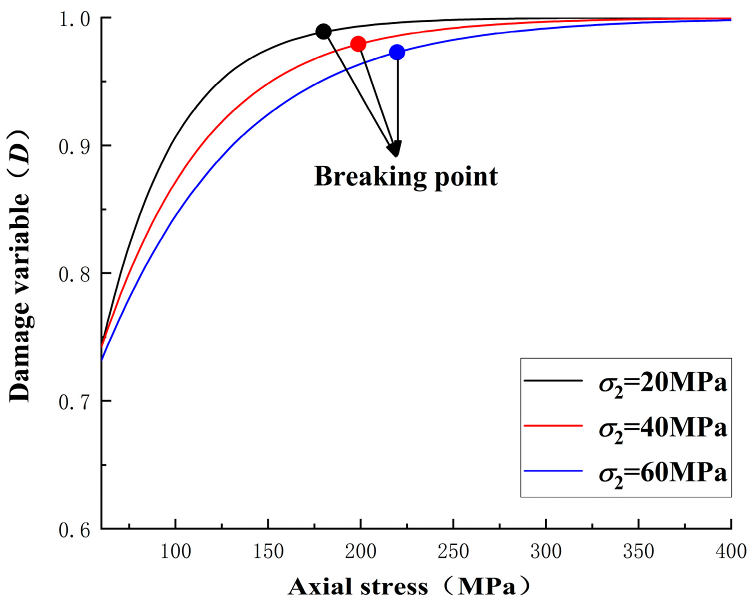

Figure 15. Damage evolution curves of sandstone under different intermediate principal stresses.

The expression of the damage variable with axial stress under different intermediate principal stresses can be obtained by substituting the formula into the following formula:

$$D = \frac{2}{\pi}\arctan[ab\exp(b\sigma_1)], \tag{11}$$

According to Figure 15, the damage variable of the sandstone increased with the increase in axial stress. In addition, the influence of intermediate principal stress on the sandstone damage variable was obvious. The lower the intermediate principal stress was, the more severe the damage evolution was and the larger the critical damage variable D_c was. This result indicates that intermediate principal stress had an inhibitory effect on the pre-peak damage of sandstone. Therefore, in the true triaxial state of sandstone, the smaller the intermediate principal stress was, the more severe the damage was. Meanwhile, the greater the intermediate principal stress was, the gentler the damage was.

4. Conclusions

The mechanical and energy evolution characteristics of sandstone under true triaxial cyclic loading were studied. The effects of different true triaxial stress paths on sandstone deformation and energy were systematically analyzed. The similarities and differences in the axial cycle under different σ_2 conditions were compared, and the energy in each principal stress direction was determined. Moreover, the dissipated energy was quantitatively analyzed, and the mechanical and damage characteristics of sandstone under true triaxial cyclic loading were revealed. The following main conclusions were derived:

1. Under the different stress paths, the axial bearing capacity and macroscopic failure characteristics of sandstone differed. The existence of confining pressure greatly improved the axial bearing capacity of the rock. The σ_1 of sandstone under a true triaxial cycle was lower than that under true triaxial compression. Under uniaxial compression, sandstone mainly experienced shear failure. During true triaxial compression, sandstone was mainly subjected to tension–shear composite failure, and in the true triaxial cycle, sandstone mainly experienced tensile failure. This showed that the rock in the true triaxial environment in the project would reduce the axial strength of the rock and change its macroscopic failure characteristics from tensile–shear composite failure to tensile failure after repeated cyclic loading.

2. In the process of true triaxial graded cyclic loading σ_1 of sandstone, the stress–strain curves and failure characteristics under different σ_2 conditions varied obviously. The larger σ_2 was, the smaller the deformation in each principal stress direction was, and the failure mode gradually changed from tensile failure to shear failure. With the increase in the load rate, σ_1, ε_v, ε_2, and ε_3 decreased when sandstone was destroyed. The expansion point was advanced, but the expansion capacity increased. The increase of σ_2 could improve the strength of rock under a true triaxial environment. The lower loading and unloading rate could reduce the damage to the rock mass and improve the safety of the project.
3. Under true triaxial cyclic loading, the input energy and elastic energy of sandstone in each principal stress direction increased nonlinearly. Similar to the direction of intermediate principal stress, in the two other principal stress directions, the dissipated energy increased nonlinearly with the increase in cyclic loading. Compared with the input energy and elastic energy in the σ_1 and σ_3 directions, the input energy and elastic energy in the σ_2 direction increased with the increase in σ_2. On the basis of the definition of the energy parameters, an energy analysis method of true triaxial graded cyclic load was proposed, which has important guiding significance for the analysis of rock dynamic disasters.
4. With graded cyclic load σ_1, the total dissipated energy of sandstone increased exponentially. Therefore, the damage variable equation was established by combining all the dissipated energies. The damage variable equation clearly described the damage evolution law of sandstone under different σ_2 values. The larger σ_2 was, the smaller the critical damage variable D_c was. Therefore, the damage of sandstone under repeated loading and unloading could be reduced by reducing σ_2.

Author Contributions: Conceptualization, C.D. and C.F.; methodology, C.F.; software, C.D.; validation, G.Z., X.L. and C.D.; formal analysis, G.Z.; investigation, R.Q. and C.F.; resources, C.D. and G.Z.; data curation, C.F.; writing—original draft preparation, C.F.; writing—review and editing, C.D.; visualization, X.L.; supervision, C.F.; project administration, M.Q.; funding acquisition, C.D. All authors have read and agreed to the published version of the manuscript.

Funding: This work is supported by the National Natural Science Foundation of China (Nos. 52074006, 51404011, 51974009, 52004005, 52004006, 52074005).

Data Availability Statement: Data sharing is not applicable.

Acknowledgments: Thanks to Fei Yang and Shuo Yang for their assistance in the experiment.

Conflicts of Interest: The authors declare no conflict of interest.

References

1. Martin, C.D.; Chandler, N.A. The progressive fracture of Lac du Bonnet granite. *Int. J. Rock Mech.* **1994**, *31*, 643–659. [CrossRef]
2. Eberhardt, E.; Stead, D.; Stimpson, B. Quantifying progressive pre-peak brittle fracture damage in rock during uniaxial compression. *Int. J. Rock Mech. Min. Sci.* **1999**, *36*, 361–380. [CrossRef]
3. Qiu, S.L.; Feng, X.T.; Xiao, J.Q.; Zhang, C.Q. An experimental study on the pre-peak unloading damage evolution of marble. *Rock Mech. Rock Eng.* **2014**, *47*, 401–419. [CrossRef]
4. Fu, J.W.; Zhang, X.Z.; Zhu, W.S.; Chen, K.; Guan, J.F. Simulating progressive failure in brittle jointed rock masses using a modified elastic-brittle model and the application. *Eng. Fract. Mech.* **2017**, *178*, 212–230. [CrossRef]
5. Yintong, G.; Kelie, Z.; Guanhua, S.; Chunhe, Y.; Hongling, M.; Guimin, Z. Experimental study of fatigue deformation and damage characteristics of salt rock under cyclic loading. *Rock Soil Mech.* **2011**, *32*, 1353–1359. (In Chinese)
6. Xiurun, G.; Yingfa, L. Discussion on fatigue failure and irreversible rock deformation under cyclic loading. *Chin. J. Geotech. Eng.* **1992**, *14*, 56–60. (In Chinese)
7. Xiurun, G.; Yu, J.; Yunde, L.; Jianxi, R. Testing study on fatigue deformation law of rock under cyclic loading. *Chin. J. Rock Mech. Eng.* **2003**, *22*, 1581–1585. (In Chinese)
8. Yongjie, Y.; Yang, S.; Jun, C. Experimental study on characteristics of strength and deformation of coal under cyclic loading. *Chin. J. Rock Mech. Eng.* **2007**, *26*, 201–205. (In Chinese)
9. Liu, E.L.; Huang, R.Q.; He, S.M. Effects of frequency on the dynamic properties of intact rock samples subjected to cyclic loading under confining pressure conditions. *Rock Mech. Rock Eng.* **2012**, *45*, 89–102. [CrossRef]

10. Fuenkajom, K.; Phueakphum, D. Effects of cyclic loading on mechanical properties of Maha Sarakham salt. *Eng. Geol.* **2010**, *112*, 43–52. [CrossRef]
11. Xiaoquan, L.; Guangzhi, Y.; Bo, C. Experimental study on deformation and seepage properties of outburst coal samples under cyclic loading. *Chin. J. Rock Mech. Eng.* **2010**, *29*, 3498–3504. (In Chinese)
12. Liu, Y.; Dai, F.; Dong, L.; Xu, N.W.; Feng, P. Experimental investigation on the fatigue mechanical properties of intermittently jointed rock models under cyclic uniaxial compression with different loading parameters. *Rock Mech. Rock Eng.* **2018**, *51*, 47–68. [CrossRef]
13. Huafeng, D.; Yu, H.; Jianlin, L.; Zhe, W.; Xiaojing, Z.; Anlong, H. The evolution of sandstone energy dissipation under cyclic loading and unloading. *Chin. J. Rock Mech. Eng.* **2016**, *35*, 2869–2875. (In Chinese)
14. Meng, Q.; Zhang, M.; Han, L.; Nie, T. Experimental research on rock energy evolution under uniaxial cyclic loading and unloading compression. *Geotech. Test. J.* **2017**, *41*, 717–729. [CrossRef]
15. Song, D.Z.; Wang, E.Y.; Liu, J. Relationship between EMR and dissipated energy of coal rock m ass during cyclic loading process. *Saf. Sci.* **2012**, *50*, 751–760. [CrossRef]
16. Dai, B.; Shan, Q.W.; Chen, Y.; Luo, X.Y. Mechanical and energy dissipation characteristics of granite under cyclic impact loading. *J. Cent. South Univ.* **2022**, *29*, 116–128. [CrossRef]
17. Moji, K. Effect of the triaxial stress system on fracture and flow of rocks. *Phys. Earth Planet. Inter.* **1972**, *5*, 318–324.
18. Baumgarten, L.; Konietzky, H. Investigations on the fracture behaviour of rocks in a triaxial compression test. In Proceedings of the ISRM International Symposium-EUROCK 2013, Wroclaw, Poland, 23–26 October 2013; pp. 861–866.
19. Ivan, P. The Strength Criterion for Rocks Under True Triaxial Stress. *Procedia Struct. Integr.* **2021**, *32*, 166–172.
20. Kwaniewski, M.; Takahashi, M.; Li, X. On the dilatant behavior of sandstone under true triaxial compression conditions. *Publ. Inst. Geophys. Pol. Acad. Sci. Ser. M. Misc.* **2002**, *24*, 321–324.
21. Gao, Y.H.; Feng, X.T. Study on damage evolution of intact and jointed marble subjected to cyclic true triaxial loading. *Eng. Fract. Mech.* **2019**, *215*, 224–234. [CrossRef]
22. Feng, X.T.; Gao, Y.H.; Zhang, X.W.; Wang, Z.F.; Zhang, Y.; Han, Q. Evolution of the mechanical and strength parameters of hard rocks in the true triaxial cyclic loading and unloading tests. *Int. J. Rock Mech. Min. Sci.* **2020**, *131*, 104349. [CrossRef]
23. Tao, W.; Yourong, L.; Zheng, H.; Chaoying, N.; Kang, W. Energy variation and damage analysis of sandstone under loading and unloading conditions in the high-stress area. *Geol. Sci. Technol. Info.* **2015**, *34*, 200–206. (In Chinese)
24. Duan, M.K.; Jiang, C.B.; Gan, Q.; Li, M.; Peng, K.; Zhang, W. Experimental investigation on the permeability, acoustic emission and energy dissipation of coal under tiered cyclic unloading (Article). *J. Nat. Gas. Sci. Eng.* **2020**, *73*, 103054. [CrossRef]
25. Minke, D.; Changbao, J.; Huan, Y.; Tian, Y.; Binwei, N.; Donglin, S. Experimental research on energy dissipation and seepage properties of coal under loading-unloading conditions at different stress levels. *Rock Soil Mech.* **2018**, *39*, 1346–1354. (In Chinese)
26. Jiang, C.B.; Duan, M.K.; Yin, G.Y.; Wang, J.G.; Xu, J.; Zhang, D.M.; Huang, G. Experimental study on seepage properties, AE characteristics, and energy dissipation of coal under tiered cyclic loading. *Eng. Geol.* **2017**, *221*, 114–123. [CrossRef]
27. Duan, M.K.; Jiang, C.B.; Yin, W.M.; Yang, K.; Li, J.Z.; Liu, Q.J. Experimental study on mechanical and damage characteristics of coal under true triaxial cyclic disturbance. *Eng. Geol.* **2021**, *295*, 106445. [CrossRef]
28. Xiaobin, Y.; Hong-ming, C.; Jiaqi, L.; Xin, H.; Chaogang, N. Energy consumption ratio evolution law of sandstones under triaxial cyclic loading. *Rock Soil Mech.* **2019**, *40*, 3751–3757. (In Chinese)
29. Luo, S.; Gong, F.Q.; Li, L.L.; Peng, K. Linear energy storage and dissipation laws and damage evolution characteristics of rock under triaxial cyclic compression with different confining pressures. *Trans. Nonferrous. Met. Soc.* **2022**, *10*, 1–26. Available online: http://kns.cnki.net/kcms/detail/43.1239.TG.20220630.1050.010.html (accessed on 8 November 2022).
30. Niu, S.J.; Ge, S.S.; Yang, D.F.; Dang, Y.H.; Yu, J.; Zhang, S. Mechanical properties and energy mechanism of saturated sandstones. *J. Cent. South Univ.* **2018**, *25*, 1447–1463. [CrossRef]
31. Li, P.; Cai, M.F. Energy evolution mechanism and failure criteria of jointed surrounding rock under uniaxial compression. *J. Cent. South Univ.* **2021**, *28*, 1857–1874. [CrossRef]
32. Ma, Q.; Tan, Y.L.; Liu, X.S.; Zhao, Z.H.; Fan, D.Y.; Purev, L. Experimental and numerical simulation of loading rate effects on failure and strain energy characteristics of coal-rock composite samples. *J. Cent. South Univ.* **2021**, *28*, 3207–3222. [CrossRef]
33. Feng, J.J.; Wang, E.Y.; Chen, X.; Ding, H.C. Energy dissipation rate: An indicator of coal deformation and failure under static and dynamic compressive loads. *Int. J. Min. Sci. Technol.* **2018**, *28*, 397–406. [CrossRef]
34. Yang, H.; Sinha, S.K.; Feng, Y.; Mccallen, D.B.; Jeremic, B. Energy dissipation analysis of elastic–plastic materials. *Comput. Methods Appl. Mech. Eng.* **2018**, *331*, 309–326. [CrossRef]
35. Jiang, X.; Bobo, L.; Ting, Z.; Dong, L.; Jie, C.; Guibing, Y. Experimental study of deformation and energy evolution law of coal under cyclic loading. *Chin. J. Rock Mech. Eng.* **2014**, *33*, 3563–3572. (In Chinese)
36. Fengnian, J.; Meirong, J.; Xiaoling, G. Defining damage variable based on energy dissipation. *Chin. J. Rock Mech. Eng.* **2004**, *23*, 1976–1980. (In Chinese)
37. Jie, L.; Jianlin, L.; Yudeng, Z.; Ting, Z.; Shanshan, Y.; Yingxia, L. Analysis of energy characteristics and deformation parameters of rock mass under cyclic loading. *Chin. J. Rock Mech. Eng.* **2010**, *29*, 3505–3513. (In Chinese)
38. Zhixi, L.; Xiangrui, M.; Guangming, Z.; Ruofei, Z.; Chongyan, L.; Siming, K.; Minjie, Q. Energy and damage analysis of sandstone under true triaxial compression. *Chin. J. Rock Mech. Eng.* **2023**, *42*, 327–341. (In Chinese)

39. Fengqiang, G.; Jingyi, Y.; Xibing, L. A new criterion of rock burst proneness based on the linear energy storage law and the residual elastic energy index. *Chin. J. Rock Mech. Eng.* **2018**, *37*, 1993–2014. (In Chinese)
40. Gong, F.Q.; Yan, J.Y.; Luo, S.; Li, X.B. Investigation on the linear energy storage and dissipation laws of rock materials under uniaxial compression. *Rock Mech. Rock Eng.* **2019**, *52*, 4237–4255. [CrossRef]
41. Gong, F.Q.; Yan, J.Y.; Li, X.B.; Luo, S. A peak-strength strain energy storage index for rock burst proneness of rock materials. *Int. J. Rock Mech. Min.* **2019**, *117*, 76–89. [CrossRef]
42. Ruidong, P.; Yang, J.; Feng, G.; Heping, X.; Peng, W. Energy analysis on damage of coal under cyclical triaxial loading and unloading conditions. *J. Chin. Coal. Soc.* **2014**, *39*, 245–252. (In Chinese)